Scalar gauge-Higgs models with discrete Abelian symmetry groups

Claudio Bonati,[1] Andrea Pelissetto,[2] and Ettore Vicari[1]
[1]*Dipartimento di Fisica, Università di Pisa, and INFN, Sezione di Pisa Largo Pontecorvo 3, I-56127 Pisa, Italy*
[2]*Dipartimento di Fisica, Università di Roma "La Sapienza", and INFN, Sezione di Roma P.le Aldo Moro 2, I-00185 Roma, Italy*

(Received 12 April 2022; accepted 6 May 2022; published 23 May 2022)

We investigate the phase diagram and the nature of the phase transitions of three-dimensional lattice gauge-Higgs models obtained by gauging the $\mathbb{Z}_N$ subgroup of the global $\mathbb{Z}_q$ invariance group of the $\mathbb{Z}_q$ clock model (N is a submultiple of q). The phase diagram is generally characterized by the presence of three different phases, separated by three distinct transition lines. We investigate the critical behavior along the two transition lines characterized by the ordering of the scalar field. Along the transition line separating the disordered-confined phase from the ordered-deconfined phase, standard arguments within the Landau-Ginzburg-Wilson framework predict that the behavior is the same as in a generic ferromagnetic model with $\mathbb{Z}_p$ global symmetry, p being the ratio q/N. Thus, continuous transitions belong to the Ising and to the O(2) universality class for $p = 2$ and $p \geqslant 4$, respectively, while for $p = 3$ only first-order transitions are possible. The results of Monte Carlo simulations confirm these predictions. There is also a second transition line, which separates two phases in which gauge fields are essentially ordered. Along this line we observe the same critical behavior as in the $\mathbb{Z}_q$ clock model, as it occurs in the absence of gauge fields.

DOI: 10.1103/PhysRevE.105.054132

I. INTRODUCTION

Classical and quantum Abelian gauge models have been extensively studied as they provide effective theories for superconductors, superfluids, and antiferromagnets [1–13]. They are also supposed to provide the effective theory for the paradigmatic example of the quantum deconfined criticality scenario [4], the transition between the Néel and the valence-bond-solid (VBS) state in two-dimensional quantum antiferromagnets; see Refs. [4,7–10] and references therein. The phase diagram and the nature of the transition lines of systems with U(1) gauge symmetry are controlled by several properties of the model. Beside the obvious dependence on the number of components of the scalar field, results depend on the charge Q of the scalar field [14–18], the explicit absence or presence of monopoles [19,20], the compact or noncompact nature of the gauge field; see, e.g., Refs. [21–23] and references therein.

In this work we study a different class of Abelian models, in which the gauge group U(1) is replaced by its subgroup $\mathbb{Z}_N$. Models with discrete local $\mathbb{Z}_2$ symmetry have been extensively studied. For instance, the $\mathbb{Z}_2$ gauge theory is the paradigmatic example of a model undergoing a topological transition, without a local order parameter [13,24,25], and is often used as a toy model to understand nonperturbative properties of lattice gauge models relevant for high-energy physics; see, e.g., Refs. [26,27]. Moreover, they are relevant to interpret critical transitions in magnetic systems [28–32] and in liquid crystals [33,34]. Models with discrete Abelian symmetries are also relevant for quantum computations. The simplest example is the $\mathbb{Z}_2$ gauge theory coupled with Ising $\mathbb{Z}_2$ spins [35–41]. Generalizations with $\mathbb{Z}_q$ scalar fields have also been considered. In the quantum setting, $\mathbb{Z}_q$ scalar fields can be realized by using parafermions [42]. When coupled with specifically engineered $\mathbb{Z}_N$ gauge fields, they may provide new routes for implementing quantum-technology devices (see Ref. [43] for a discussion and a list of relevant references).

To define the model that we consider, we start from the $\mathbb{Z}_q$ clock model, in which the scalar fields are phases that take q discrete values, and we gauge the $\mathbb{Z}_N$ subgroup of the invariance symmetry group $\mathbb{Z}_q$. Models with global $\mathbb{Z}_q$ symmetry occur in several contexts and have attracted significant interest in recent years because of their connection with the Néel-VBS transition in antiferromagnets; see Refs. [44–47] and references therein. In the absence of gauge fields, for $q \geqslant 4$, one observes the phenomenon of symmetry enlargement at the transition. Large-scale universal properties become O(2) invariant, the $\mathbb{Z}_q$ anisotropy playing the role of a dangerously irrelevant operator. It is important to stress that models with discrete gauge and global symmetry groups are also relevant in view of their possible realization using cold-atom quantum technology. Indeed, in this framework it is essential that the Hilbert space be finite. Possible implementations of $\mathbb{Z}_2$ gauge systems have recently been proposed; see, e.g., Ref. [48]. Moreover, the discretization of the scalar degrees of freedom leads to faster classical and quantum computations [49–52].

In this work we investigate the role that the gauge symmetry group plays in determining the phase diagram and the nature of the transition lines. We find that all transition lines where the matter fields show long-range correlations can be interpreted in terms of an effective Landau-Ginzburg-Wilson theory in which one only considers the dynamics of a scalar order parameter. As a consequence, the universality class of

the transitions only depends on the global symmetry group and on the discrete nature of the scalar field. A second, important issue is the question of the symmetry enlargement at the transition. In other words, we would like to determine under which conditions one can observe the O(2) critical behavior in the presence of $\mathbb{Z}_N$ local invariance. As we shall see, it also occurs in the gauged model for $p = q/N \geqslant 4$.

The paper is organized as follows. In Sec. II we define the model, while in Sec. III we specify the quantities that are determined in the Monte Carlo simulations. The expected phase diagram is discussed in Sec. IV, while the numerical results are presented in Sec. V. Finally, in Sec. VI we summarize the results and draw our conclusions. In the Appendices we report some useful results. In Appendices A and B we report exact results for the $\mathbb{Z}_4$ and $\mathbb{Z}_8$ models with $\mathbb{Z}_2$ gauge invariance. In Appendix C we compute the relevant scaling functions for the Ising and the XY model that are compared with the numerical results in Sec. V.

II. THE MODEL

We consider a $\mathbb{Z}_N$ gauge model coupled with a complex scalar field defined on a cubic lattice. The fundamental fields are complex phases $w_{\boldsymbol{x}}$, satisfying $|w_{\boldsymbol{x}}| = 1$, associated with the sites of the lattice and phases $\sigma_{\boldsymbol{x},\mu}$, $|\sigma_{\boldsymbol{x},\mu}| = 1$, associated with the lattice links. These phases can only take q and N values, respectively, where q is an integer multiple of N. More precisely, we set

$$w = \exp(2\pi i m/q), \quad \sigma = \exp(2\pi i n/N), \tag{1}$$

where $m = 0, \ldots, q-1$, $n = 0, 1 \ldots N-1$.

The corresponding Hamiltonian is defined as

$$H = H_{\rm kin} + H_{\rm g}. \tag{2}$$

The first term is

$$H_{\rm kin} = -J\ {\rm Re} \sum_{\boldsymbol{x},\mu} \bar{w}_{\boldsymbol{x}} \sigma_{\boldsymbol{x},\mu}\, w_{\boldsymbol{x}+\hat{\mu}}, \tag{3}$$

where the sum is over all lattice sites $\boldsymbol{x}$ and directions μ ($\hat{\mu}$ are the corresponding unit vectors). The second term is

$$H_{\rm g} = -g \sum_{\boldsymbol{x},\mu>\nu} {\rm Re}\ \Pi_{\boldsymbol{x},\mu\nu}, \tag{4}$$

where the sum is over all lattice plaquettes, and the plaquette contribution is given by

$$\Pi_{\boldsymbol{x},\mu\nu} = \sigma_{\boldsymbol{x},\mu} \sigma_{\boldsymbol{x}+\hat{\mu},\nu} \bar{\sigma}_{\boldsymbol{x}+\hat{\nu},\mu} \bar{\sigma}_{\boldsymbol{x},\nu}. \tag{5}$$

The partition function is

$$Z = \sum_{z,\sigma} e^{-H/T}. \tag{6}$$

In the following we use $\beta = J/T$ and $\kappa = g/T$ as independent variables. The model is invariant under local $\mathbb{Z}_N$ and global $\mathbb{Z}_q$ transformations. The global symmetry group is $\mathbb{Z}_q/\mathbb{Z}_N = \mathbb{Z}_p$ with

$$p = \frac{q}{N}. \tag{7}$$

The model is well defined also if N is unrelated to q, but in this case it is only invariant under $\mathbb{Z}_M$ local transformations, where M is the greatest common divisor of N and q. If N is an integer multiple of q, then the model is invariant under local $\mathbb{Z}_q$ transformations and it is possible to integrate out the scalar fields, performing the change of variable $\tau_{\boldsymbol{x},\mu} = \sigma_{\boldsymbol{x},\mu} \bar{w}_{\boldsymbol{x}} w_{\boldsymbol{x}+\hat{\mu}}$. One obtains the Hamiltonian of a $\mathbb{Z}_N$ gauge model in the presence of a linear gauge-symmetry breaking term,

$$H = -g \sum_{\boldsymbol{x},\mu>\nu} \Pi_{\boldsymbol{x},\mu\nu} - J\ {\rm Re} \sum_{\boldsymbol{x},\mu} \tau_{\boldsymbol{x},\mu}, \tag{8}$$

where the plaquette is expressed in terms of the new field τ. For $N = q = 2$ this model has been extensively studied [26,27,32,35–41]. Here we shall focus on the case $q > N$.

III. THE OBSERVABLES

In our numerical study we consider cubic lattices of linear size L. As we are dealing with topological transitions, one should carefully choose the boundary conditions. We consider open boundary conditions, to avoid slowly decaying dynamic modes that are present in systems with periodic boundary conditions. Indeed, in the latter case, the Polyakov loops (the product of the gauge compact fields along nontrivial lattice paths that wrap around the lattice) have a very slow dynamics, especially in the gauge deconfined phase, if one uses algorithms with local updates. For open boundary conditions, Polyakov loops are not gauge invariant and thus their dynamics is not relevant for the estimation of gauge-invariant observables. A local algorithm is therefore efficient. Of course, open boundary conditions give rise to additional scaling corrections, due to the boundary, and thus larger systems are needed to obtain asymptotic results.

We simulate the system using a standard Metropolis algorithm. We compute the energy densities and the specific heats

$$\begin{aligned} E_k &= \frac{1}{V}\langle H_{\rm kin}\rangle, \quad C_k = \frac{1}{V}\left(\langle H_{\rm kin}^2\rangle - \langle H_{\rm kin}\rangle^2\right), \\ E_g &= \frac{1}{V}\langle H_{\rm g}\rangle, \quad C_g = \frac{1}{V}\left(\langle H_{\rm g}^2\rangle - \langle H_{\rm g}\rangle^2\right), \end{aligned} \tag{9}$$

where $V = L^3$.

We consider the two-point correlation function of the field w with charge Q:

$$\begin{aligned} G_Q(\boldsymbol{x},\boldsymbol{y}) &= {\rm Re}\,\langle (\bar{w}_{\boldsymbol{x}} w_{\boldsymbol{y}})^Q\rangle, \\ &= \langle \cos\left[2\pi Q(m_{\boldsymbol{x}} - m_{\boldsymbol{y}})/q\right]\rangle, \end{aligned} \tag{10}$$

where $m_{\boldsymbol{x}}$ is defined in Eq. (1). If Q is a multiple of N, then the correlation function $G_Q(\boldsymbol{x},\boldsymbol{y})$ is gauge invariant. Then, we define the Fourier transform

$$\widetilde{G}_Q(\boldsymbol{p}) = \frac{1}{V} \sum_{\boldsymbol{x},\boldsymbol{y}} e^{i\boldsymbol{p}\cdot(\boldsymbol{x}-\boldsymbol{y})} G_Q(\boldsymbol{x},\boldsymbol{y}) \tag{11}$$

(V is the volume), and the corresponding susceptibility and correlation length,

$$\chi_Q = \widetilde{G}_Q(\boldsymbol{0}), \tag{12}$$

$$\xi_Q^2 \equiv \frac{1}{4\sin^2(\pi/L)} \frac{\widetilde{G}_Q(\boldsymbol{0}) - \widetilde{G}_Q(\boldsymbol{p}_m)}{\widetilde{G}_Q(\boldsymbol{p}_m)}, \tag{13}$$

where $\boldsymbol{p}_m = (2\pi/L, 0, 0)$. Note that, since we use open boundary conditions, the choice of $\boldsymbol{p}_m$ is somewhat arbitrary.

Other choices, as long as they satisfy $|p_m| \sim 1/L$, would be equally valid.

In our FSS analysis we use renormalization-group invariant quantities. We consider

$$R_{\xi,Q} = \xi_Q/L, \tag{14}$$

and the charge-Q Binder parameter

$$U_Q = \frac{\langle \mu_{2,Q}^2 \rangle}{\langle \mu_{2,Q} \rangle^2}, \quad \mu_{2,Q} = \sum_{\boldsymbol{xy}} \mathrm{Re}\,(\bar{w}_{\boldsymbol{x}} w_{\boldsymbol{y}})^Q. \tag{15}$$

To determine the nature of the transition, one can consider the L dependence of the maximum $C_{\max}(L)$ of one of the specific heats. At a first-order transition, $C_{\max}(L)$ is proportional to the volume L^3, while at a continuous transition it behaves as

$$C_{\max}(L) = aL^{\alpha/\nu} + C_{\mathrm{reg}}. \tag{16}$$

The constant term C_{reg}, due to the analytic background, is the dominant contribution if $\alpha < 0$. The analysis of the L-dependence of $C_{\max}(L)$ may allow one to distinguish first-order and continuous transitions. However, experience with models that undergo weak first-order transitions indicates that in many cases the analysis of the specific heat is not conclusive. The maximum $C_{\max}(L)$ may start scaling as L^3 at values of L that are much larger than those at which simulations can be actually performed. A more useful quantity is a Binder parameter U, which has a qualitatively different behavior at continuous and first-order transitions. In the latter case, the maximum $U_{\max}(L)$ of U at fixed size L increases with the volume [53,54]. On the other hand, U is bounded as $L \to \infty$ at a continuous phase transition. In this case, in the FSS limit, any renormalization-group invariant quantity R scales as

$$\begin{aligned} R(\beta, L) &\approx f_R(X) + L^{-\omega} f_{c,R}(X), \\ X &= (\beta - \beta_c) L^{1/\nu}, \end{aligned} \tag{17}$$

where ω is a correction-to-scaling exponent. Thus, a first-order transition can be identified by verifying that $U_{\max}(L)$ increases with L, without the need of explicitly observing the linear behavior in the volume.

In the case of weak first-order transitions, the nature of the transition can also be understood from the combined analysis of U and R_ξ. At a continuous transition, in the FSS limit any renormalization-group invariant quantity R scales as

$$R(\beta, L) = F_R(R_\xi) + L^{-\omega} F_{c,R}(R_\xi) + \ldots, \tag{18}$$

where $F_R(x)$ is universal and $F_{c,R}(x)$ is universal apart from a multiplicative constant. The Binder parameter U does not obey this scaling relation at first-order transitions, because of the divergence of U for $L \to \infty$. Therefore, the order of the transition can be understood from plots of U versus R_ξ. The absence of a data collapse is an early indication of the first-order nature of the transition.

IV. PREDICTED PHASE DIAGRAM

Our simulations are consistent, as we shall see in Sec. V, with the phase diagram shown in Fig. 1, with three different phases. To clarify their nature and the universality class of the different transition lines, it is useful to discuss some limiting cases.

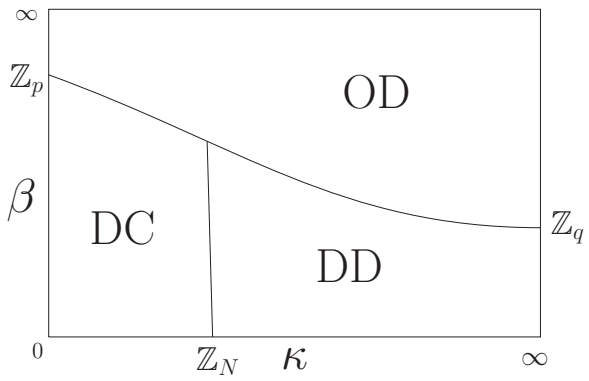

FIG. 1. Phase diagram of the model. Three phases are present: a disorderd-confined (DC) phase, a disordered-deconfined (DD) phase, and an ordered-deconfined (OD) phase. For $\kappa = 0$ there is a ferromagnetic $\mathbb{Z}_p$ ($p = q/N$) transition, for $\beta = 0$ a topological $\mathbb{Z}_N$ transition, and for $\kappa \to \infty$ a ferromagnetic $\mathbb{Z}_q$ transition.

In the limit $\kappa \to \infty$, the gauge degrees of freedom freeze and one can set $\sigma_{\boldsymbol{x},\mu} = 1$ on all links (when open boudary conditions are used this is also true in a finite volume), obtaining the ferromagnetic $\mathbb{Z}_q$ clock model, which undergoes a standard finite-β transition. For $q = 2$ and 4 it belongs to the Ising universality class, for $q = 3$ it is of first order, while for $q \geqslant 5$ the critical behavior is the same as in the XY model, see Refs. [45,47,49].

Note that a $\mathbb{Z}_q$ perturbation is irrelevant [55] at the XY fixed point for any $q \geqslant 4$ and, in particular, also for $q = 4$. Thus, XY critical behavior is generically expected in models with $\mathbb{Z}_4$ global invariance and it has been indeed observed in systems with soft $\mathbb{Z}_4$ breakings [46,56]. The standard $\mathbb{Z}_4$ clock model, which undergoes an Ising transition [45], is an exception. It behaves differently, because the model can be formulated in terms of two decoupled Ising spins on each site. In generic $\mathbb{Z}_4$ systems with discrete fields, one can still parametrize the model in terms of two Ising spins, but now they are coupled by an energy-energy interaction. At the decoupled Ising fixed point, this perturbation is relevant, although with a rather small renormalization-group dimension [55] given by $2/\nu_{\mathrm{Is}} - 3 = 0.17475(2)$, if we use the estimate $\nu_{\mathrm{Is}} = 0.629971(4)$ of the Ising-model exponent [57]. The energy-energy interaction is the one that drives the system towards the XY fixed point, if the transition is continuous.

For $\beta = 0$, there are no scalar fields and one obtains a pure gauge $\mathbb{Z}_N$ model, that can be related by duality [44] to a $\mathbb{Z}_N$ spin model, with a global $\mathbb{Z}_N$ symmetry. The $\mathbb{Z}_N$ gauge theory undergoes a topological transition at κ_c, which belongs to the same universality class as the corresponding transition in the $\mathbb{Z}_N$ spin clock model. Estimates of κ_c can be found in Ref. [58]. For $N = 2$, we can use the results of Ref. [59] for the standard Ising model and duality to estimate $\kappa_c = 0.761413292(12)$. For $N \to \infty$, one has [18,58]

$$\kappa_c \simeq \kappa_{gc} N^2, \tag{19}$$

where $\kappa_{gc} = 0.076051(2)$ is the critical coupling of the inverted XY model [60].

For $\kappa = 0$, one can sum over the gauge fields and obtain a gauge-invariant Hamiltonian that depends on the fields $w_{\boldsymbol{x}}$ only. For generic values of N, the expression of the effective Hamiltonian is complex and not very illuminating. However, one expects the same critical behavior for any local Hamiltonian that is invariant under local $\mathbb{Z}_N$ transformations. One such Hamiltonian is

$$H_{\rm eff} = -J \sum_{\boldsymbol{x},\mu} {\rm Re}\, (\bar{w}_{\boldsymbol{x}+\hat{\mu}} w_{\boldsymbol{x}})^N$$
$$= -J \sum_{\boldsymbol{x},\mu} \cos\left[\frac{2\pi N}{q}(m_{\boldsymbol{x}+\hat{\mu}} - m_{\boldsymbol{x}})\right]. \qquad (20)$$

If we express $m_{\boldsymbol{x}} = p n_{1,\boldsymbol{x}} + n_{2,\boldsymbol{x}}$, with $n_{1,\boldsymbol{x}} = 0, \ldots N-1$, $n_{2,\boldsymbol{x}} = 0, \ldots p-1$ ($p = q/N$), then we obtain the Hamiltonian of a ferromagnetic $\mathbb{Z}_p$ clock model (the Ising model for $p = 2$). Analogously, the correlation function $G_N(\boldsymbol{x}, \boldsymbol{y})$ in the model with Hamiltonian Eq. (20) is equivalent the correlation function $G_1(\boldsymbol{x}, \boldsymbol{y})$ in the $\mathbb{Z}_p$ clock model. For $N = 2$ and $q = 4$, one can show that the Hamiltonian Eq. (2) is exactly equivalent to Eq. (20) for $\kappa = 0$, see Appendix A, and thus, in this case, the relation of the gauge model with the Ising model is exact.

On the basis of the previous argument we predict the universality class of the transition at $\kappa = 0$ to depend only on the ratio $p = q/N$, and to be the same as that of the $\mathbb{Z}_p$ clock model (as we discuss below, for $p \neq 4$). Therefore, if the transitions are continuous, then they should belong to the Ising universality class for $p = 2$ and to the XY universality class for $p \geqslant 5$. For $p = 3$, instead, we expect a discontinuous transition as in the $\mathbb{Z}_3$ clock model. For $p = 4$, the transition in the $\mathbb{Z}_4$ clock model is not the generic one expected in $\mathbb{Z}_4$ invariant systems. In Appendix B we have performed an exact calculation for the $\mathbb{Z}_8$ model with $\mathbb{Z}_2$ gauge invariance. For $\kappa = 0$, the model can be rewritten in terms of two Ising spins $\rho_{\boldsymbol{x}}^{(1)}$ and $\rho_{\boldsymbol{x}}^{(2)}$, with Hamiltonian

$$H_{\rm eff} = \sum_{\boldsymbol{x},\mu} \left[B(\beta)\rho_{\boldsymbol{x}}^{(1)}\rho_{\boldsymbol{x}+\hat{\mu}}^{(1)} + B(\beta)\rho_{\boldsymbol{x}}^{(2)}\rho_{\boldsymbol{x}+\hat{\mu}}^{(2)} + C(\beta)\rho_{\boldsymbol{x}}^{(1)}\rho_{\boldsymbol{x}+\hat{\mu}}^{(1)}\rho_{\boldsymbol{x}}^{(2)}\rho_{\boldsymbol{x}+\hat{\mu}}^{(2)}\right], \qquad (21)$$

where the functions $B(\beta)$ and $C(\beta)$ can be derived using the results of Appendix B. The decoupling of the two Ising systems that occurs in the $\mathbb{Z}_4$ clock model does not occur here [$C(\beta)$ does not vanish] and therefore we expect XY behavior, if the transition is continuous. The same result is expected for any q and any N, with $p = 4$.

Finally, several results [34] are available for $N = 2$ in the limit $q \to \infty$, in which $w_{\boldsymbol{x}}$ is an unconstrained phase and the global invariance group is U(1). The phase diagram is similar to the one reported in Fig. 1. There are three different phases that can be characterized by the behavior of the gauge and scalar degrees of freedom [34]. For small β and κ, gauge modes are confined, while they are deconfined in the other two phases. As for the scalar degrees of freedom, they are disordered in the two small-β phases, while they are ordered (the $\mathbb{Z}_q$ symmetry is broken) in the large-β phase. The three phases are separated by three transition lines. Along the transition lines that separate the large-β ordered-deconfined (OD) phase from the two low-β phases, transitions belong [34] to the XY universality class, as in the models obtained for $\kappa \to 0$ and $\kappa \to \infty$. Along the line that separates the disorderd-confined (DC) phase from the disordered-deconfined (DD) phase one expects the same behavior as in the $\mathbb{Z}_N$ gauge model obtained for $\beta = 0$.

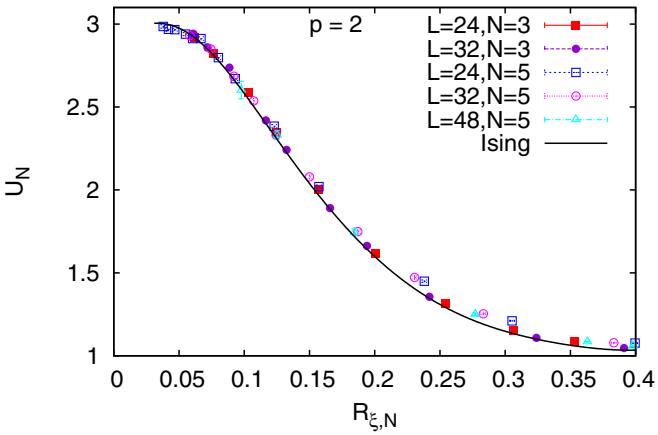

FIG. 2. Estimates of U_N versus $R_{\xi,N}$ for the models with $N = 3$, $q = 6$ and with $N = 5$, $q = 10$, at fixed $\kappa = 0.4$. In both cases $p = q/N = 2$. We also report the universal curve $F_{\xi,1}(R_{\xi,N})$ computed in the Ising model ("Ising").

It is conceivable, and we shall verify it in the next section, that the same phase diagram holds for the models we consider here as long as $q > N$. Moreover, as in the case $q = \infty$, we expect the critical behavior along the three lines to be the same as at the corresponding endpoint at $\beta = 0$, $\kappa = 0$, and $\kappa \to \infty$. The only exceptions might occur for $N = 4$, along the DC-DD line and for $q = 4$ along the DD-OD line. In these cases, it is *a priori* possible to observe XY behavior instead of Ising behavior. However, since the crossover exponent of the relevant perturbation that drives the system out of the decoupled Ising fixed point is rather small [55], significant crossover effects may be present.

V. NUMERICAL RESULTS

A. Small-κ transition line

Let us now discuss the behavior along the DC-OD transition line. For this purpose we have performed simulations at fixed κ, varying β. In all cases, we set $\kappa = 0.4$, which, on the basis of the estimates of κ_c at $\beta = 0$ reported in Ref. [58], should guarantee that we are studying a transition belonging to the DC-OD line. As we mentioned, we expect the phase behavior to depend only on $p = q/N$.

1. Models with $p = 2$

For $p = 2$ we have performed simulations for $(q, N) = (4, 2)$, $(6, 3)$, and $(10,5)$. In Fig. 2 we report we report U_N versus $R_{\xi,N} = \xi_N/L$ for $N = 3$ and 5, together with the scaling function $F_{U,1}(R_{\xi,N})$, where $F_{U,1}(x)$ is the asymptotic scaling function that expresses U_1 in terms of $R_{\xi,1}$ in the Ising model (the computation is discussed in Appendix C). For $N = 3$, the data essentially fall on top of the Ising scaling curve, while the results for $N = 5$ show tiny deviations that decrease as L increases. To provide a better check that the asymptotic

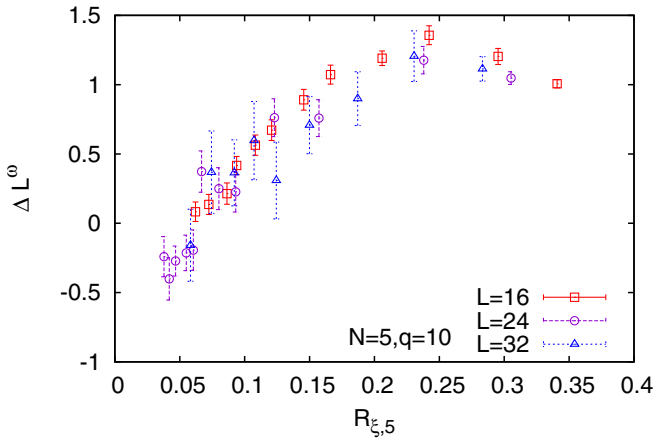

FIG. 3. Estimates of $L^{\omega}\Delta$ versus $R_{\xi,N}$ for $N = 5$, $q = 10$ ($p = q/N = 2$), at fixed $\kappa = 0.4$. The function Δ is defined in Eq. (22). We use the correction-to-scaling exponent for Ising systems, $\omega = 0.83$.

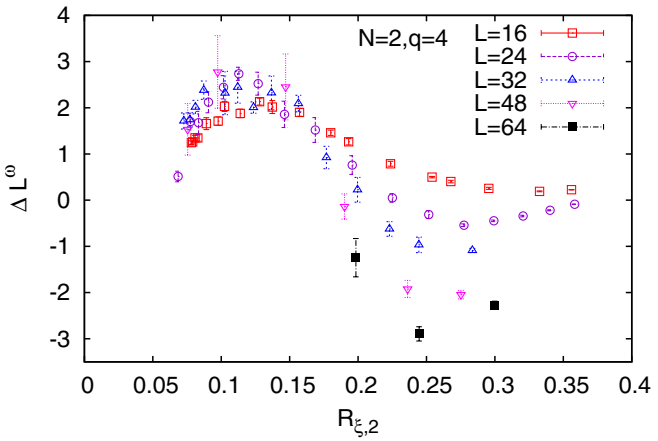

FIG. 5. Estimates of $L^{\omega}\Delta$ versus $R_{\xi,2}$ for $N = 2$, $q = 4$ at fixed $\kappa = 0.4$. The function Δ is defined in Eq. (22). We use the correction-to-scaling exponent for Ising systems, $\omega = 0.83$.

behavior for $N = 5$ is the same as in the Ising model, we have determined the corrections, defining

$$\Delta(R_{\xi,N}) = U_N - F_{U,1}(R_{\xi,N}). \tag{22}$$

If the transition belongs to the Ising universality class, then the estimates of $L^{\omega}\Delta(R_{\xi,N})$ should approximately belong to a single curve, provided one uses $\omega = 0.8303(18)$, which is the correction-to-scaling exponent for the Ising universality class [57,61]. The results are shown in Fig. 3. For $N = 5$, $q = 10$ we observe a nice scaling. Moreover, as expected, the shape of the curve is similar to that observed for the Ising model, see Appendix C.

As an additional check, we have performed combined fits of U_N and $R_{\xi,N}$ to Eq. (17), parametrizing $f_R(x)$ and $f_{c,R}(x)$ with polynomials. If we let ν be a free parameter and fix $\omega = 0.83$ (the value for the Ising universality class), then we obtain $\nu = 0.62(1)$ ($N = 3$) and $0.64(1)$ ($N = 5$). These results are consistent with the Ising prediction $\nu = 0.629971(4)$ [57,61]. To estimate the position of the critical point, we have then performed fits fixing $\nu = 0.629971$. We obtain $\beta_c = 1.4546(1)$ and $\beta_c = 4.5660(7)$ for $N = 3$ and $N = 5$, respectively.

Finally, we consider the case $N = 2$ and $q = 4$. The estimates of U_2 versus $R_{\xi,2}$ are reported in Fig. 4. Data are close to the Ising curve. However, at a closer look, deviations from the Ising curve do not decrease as L increases. This is evident from Fig. 5, where we report the deviations from the Ising curve. For $0.2 \lesssim R_{\xi,2} \lesssim 0.35$ deviations apparently increase as L increases.

To clarify the nature of the transition, we have analyzed U_2 and $R_{\xi,2}$ as a function of $X = (\beta - \beta_c)L^{1/\nu}$. Again, results are not consistent with an Ising behavior. Indeed, repeating the combined analysis of U_N and $R_{\xi,N}$, as we did before, we obtain $\nu = 0.56(1)$ if we consider all data, and $\nu = 0.54(1)$, if only results with $L \geqslant 24$ are included. Additional information on the critical behavior is provided by the analysis of the specific heats C_g and C_k. They have a pronounced peak that increases with L, see Fig. 6 for a plot of C_k. The maximum increases apparently as $L^{0.8}$, much more than in the Ising model, in which it increases as $L^{\alpha/\nu}$ with $\alpha/\nu \approx 0.17$. Finally, we compute the

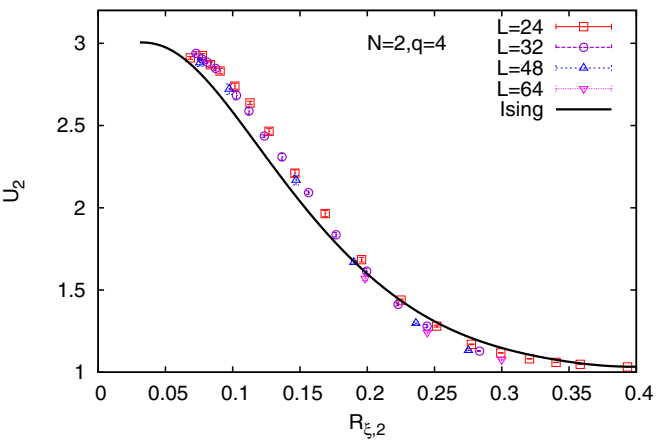

FIG. 4. Estimates of U_2 versus $R_{\xi,2}$ for the model with $N = 2$, $q = 4$ at fixed $\kappa = 0.4$. Results are compared with the scaling function computed in the Ising model, as in Fig. 2.

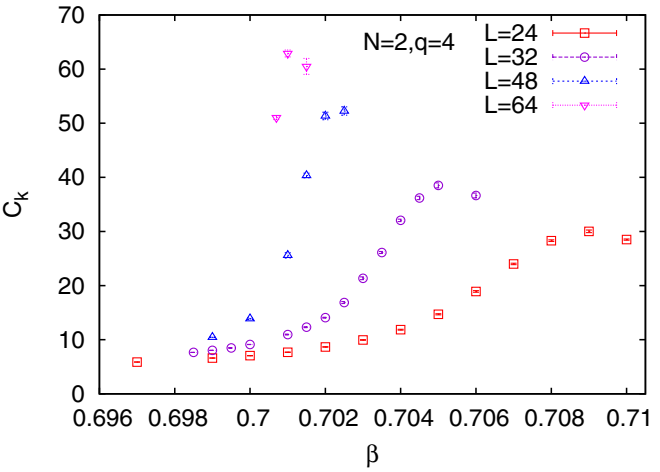

FIG. 6. Estimates of the specific heat C_k versus β for $N = 2$, $q = 4$ at fixed $\kappa = 0.4$.

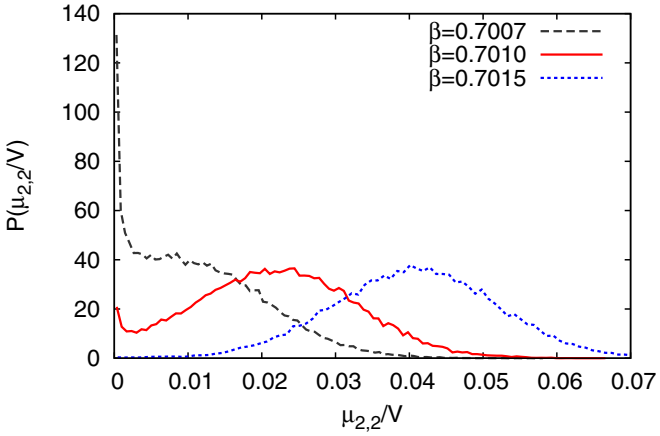

FIG. 7. Probability distribution of the order parameter $\mu_{2,2}/V$ ($V = L^3$ is the volume) for the model with $N = 2$, $q = 4$. Results for $\beta = 0.7007, 0.7010, 0.7015$ at fixed $\kappa = 0.4$. Here $L = 64$.

distributions of the order parameter $\mu_{2,2}$ defined in Eq. (15). In Fig. 7 we report the results for three values of β and for lattices of size $L = 64$. For $\beta = 0.7010$ we observe the presence of two maxima, a hint for a first-order transition: a very sharp one for $\mu_{2,2} \approx 0$ and a broad one at a finite value of $\mu_{2,2}$.

Collecting all results we conclude that the critical behavior along the DC-OD transition line for $N = 2$ is not the same as for $N \geqslant 3$. The most likely possibility is that the Ising transition that occurs for $\kappa = 0$ (for this value of the gauge coupling, the model can be mapped exactly onto the Ising model, see Appendix A) turns into a first-order transition at some critical value κ^*: for $\kappa < \kappa^*$ we have an Ising transition, for $\kappa > \kappa^*$ the transition becomes of first order, while for $\kappa = \kappa^*$ there is a tricritical point with mean-field exponents (in particular, $\nu = 1/2$) with logarithmic corrections. We are not able to estimate κ^*. We can only infer from the data that κ^* should be smaller than, but not very much different from, $\kappa = 0.4$, the value at which simulations have been performed. Indeed, the numerical data in Fig. 4 are close to the Ising universal curve, indicating the presence of strong Ising crossover effects that can be explained by the presence of a nearby Ising transition line. Moreover, the estimates of the critical exponent ν and of the specific-heat exponent α/ν are not far from the values expected for a tricritical point, $\nu = 1/2$ and $\alpha/\nu = 1$.

The present results can also be used to predict the behavior of two Ising systems that interact by means of a $\mathbb{Z}_2$ gauge field (this is the equivalent interpretation of the $\mathbb{Z}_4$ model with $\mathbb{Z}_2$ gauge invariance, see Appendix A). The gauge interaction, if sufficiently strong, is able to drive the system far from the Ising fixed point, giving rise to a first-order transition.

2. Models with $p = 3$

For $p = 3$ we have performed simulations for $(q, N) = (6, 2)$ and (9,3). As expected, in all cases data suggest a first-order transition, at $\beta_c \approx 0.875$ and $\beta_c \approx 1.89$, respectively, as in the $\mathbb{Z}_3$ model. To clarify the nature of the critical behavior, we have studied the behavior of the Binder parameters U_N as a function of $R_{\xi,N}$. The results for the two models are reported in Fig. 8. In both cases, we do not observe scaling. As L increases, the estimates of U_N at fixed $R_{\xi,N}$ apparently

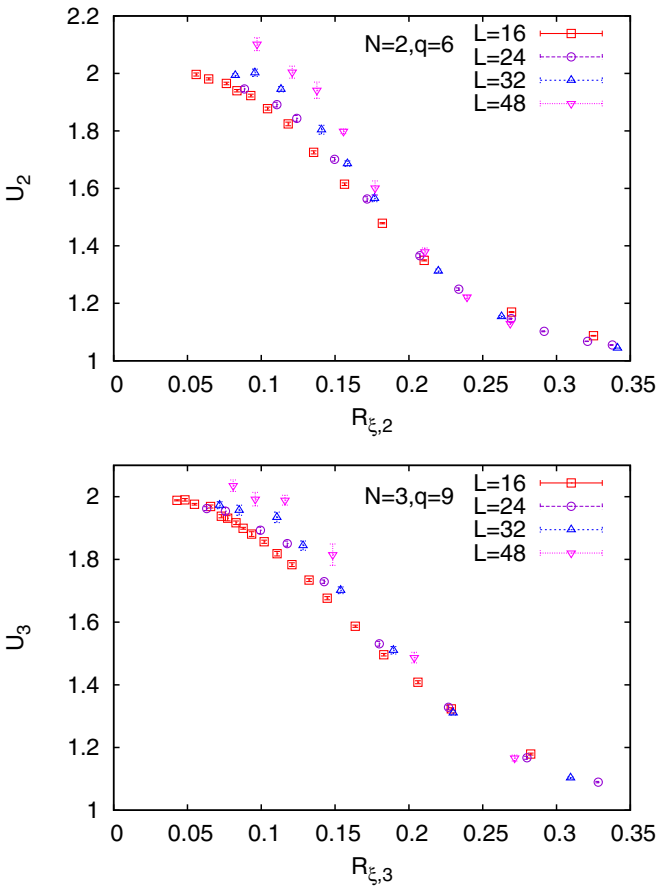

FIG. 8. Estimates of U_N versus $R_{\xi,N}$ for $N = 2$, $q = 6$ (top) and $N = 3$, $q = 9$ (bottom), at fixed $\kappa = 0.4$. In both cases $p = q/N = 3$.

increase, especially for $0.07 \lesssim R_{\xi,N} \lesssim 0.15$. In particular, the maximum $U_{\max}(L)$ slightly increases as a function of L. These results are all consistent with a first-order transition. It is clear that a convincing identification of the first-order nature of the transition requires significantly larger lattices. However, given that these conclusions are already in agreement with what is expected on the basis of the arguments of Sec. IV, we have not further pursued this issue.

3. Models with $p \geqslant 4$

For $p = 4$ we have performed simulations for $(q, N) = (8, 2)$ and (12,3), while for $p = 5$ we have performed simulations for $(q, N) = (10, 2)$ and (15,3). For both values of p, data are consistent with an XY behavior; see Fig. 9. While for $p = 5$ this is the same behavior as observed in the $\mathbb{Z}_5$ model, for $p = 4$ we do not observe the Ising behavior characterizing the clock $\mathbb{Z}_4$ model. On the one side, this is expected, since in generic models with $\mathbb{Z}_4$ symmetry breaking one expects the emergence of an enlarged O(2) symmetry. On the other side, it is somewhat surprising to observe such a good agreement, given that we expect very slowly-decaying corrections (behaving approximately as $L^{-0.1}$) due to the spin-four operator that breaks the O(2) symmetry down to $\mathbb{Z}_4$. We have no evidence of such corrections in the plots of U_N versus $R_{\xi,N}$.

To estimate the critical point β_c we have performed fits to Eq. (17). Assuming the transition to belong to the XY

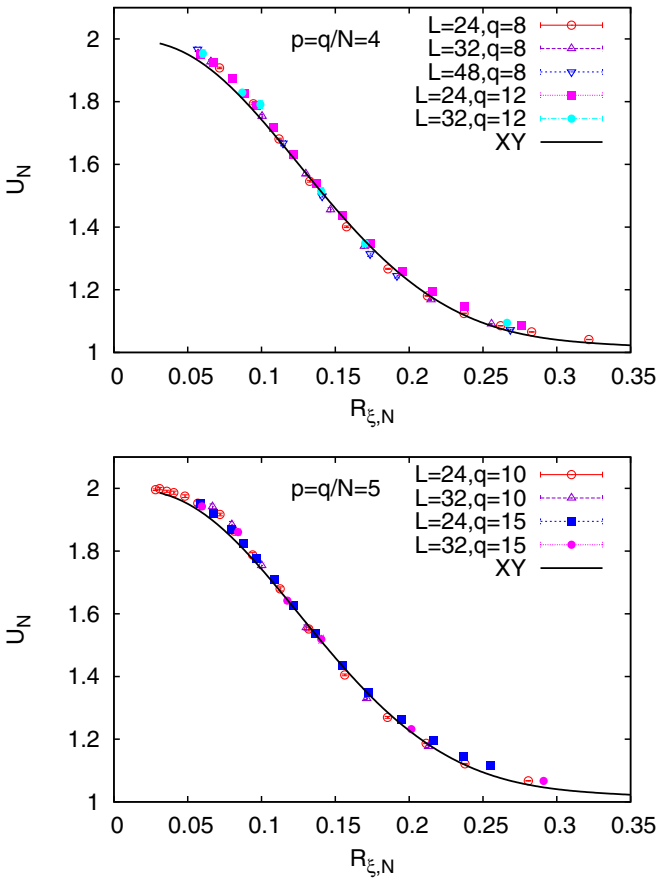

FIG. 9. Estimates of U_N versus $R_{\xi,N}$ for $N = 2$, $q = 8$ and $N = 3$, $q = 12$ (data with $p = 4$, top) and for $N = 2$, $q = 10$ and $N = 3$, $q = 15$ (data with $p = 5$, bottom), at fixed $\kappa = 0.4$. Results are compared with the scaling function appropriate for the XY universality class, see Appendix C.

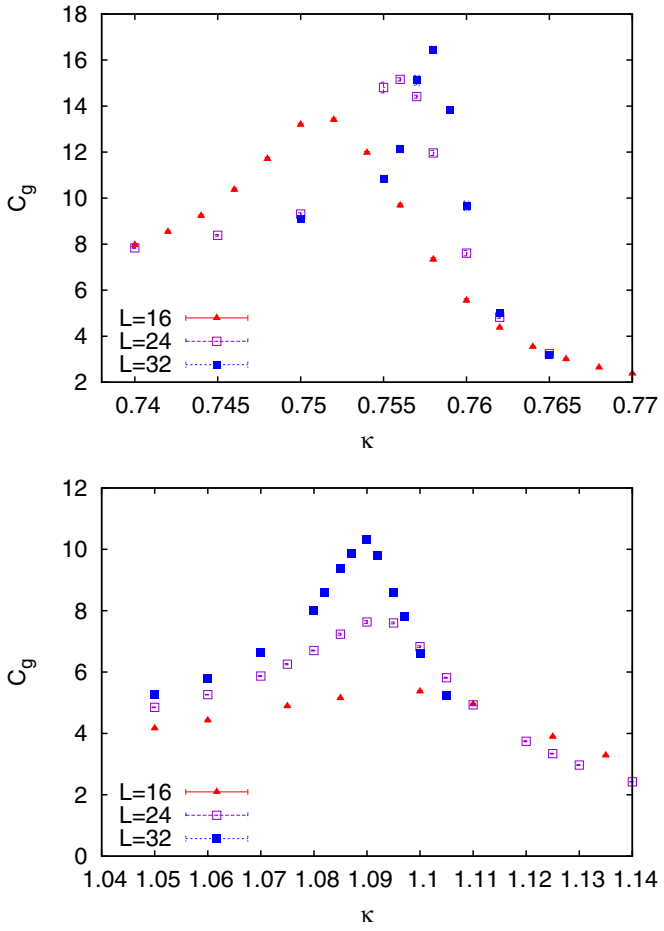

FIG. 10. Estimates of the gauge specific heat C_g as a function of κ at fixed $\beta = 0.2$. Top: results for $N = 2$ and $q = 6$. Bottom: results for $N = 3$ and $q = 9$. An extrapolation of the position $\beta_{\max}$ of the maximum of C_g (we use $\beta_{\max} = \beta_c + bL^{-s}$, with $s = 1/\nu_{\rm Ising} = 1.59$ for $N = 2$ and with $s = d = 3$ for $N = 3$) gives $\beta_c \approx 0.76$ and $\beta_c \approx 1.08$ for $N = 2$ and 3, respectively.

universality class, we have fixed $\nu = 0.6717$ and $\omega = 0.789$ [49,62,63]. Results show a very tiny dependence on q. For $N = 2$ we obtain $\beta_c = 0.8869(1)$ and $0.8869(2)$ for $q = 8$ and 10, respectively. For $N = 3$, we have $\beta_c = 1.9160(15)$, $1.9150(15)$ for $q = 12$ and 15.

4. Summary and Landau-Ginzburg-Wilson effective theory

The numerical simulations confirm the predictions of Sec. IV. The only relevant variable along the DC-OD line is the ratio $p = q/N$. For $p = 2$ we confirm that the models belong to the Ising universality class, with one only exception, the model with $q = 4$ and $N = 2$, which undergoes a first-order transition, at least for not too small values of κ. For $p = 3$, the transition is apparently of first order, as in the $\mathbb{Z}_3$ clock model. For $p \geqslant 4$, we observe XY behavior in all cases, including $p = 4$. Note that in the latter case the $\mathbb{Z}_4$ clock model has an Ising transition due to a peculiar factorization of the degrees of freedom, see Appendix A.

These results have a very simple interpretation in the Landau-Ginzburg-Wilson (LGW) framework. In this approach, one assumes that the critical behavior is completely determined by the gauge-invariant scalar modes, so that it can be determined by considering a gauge-invariant order parameter and studying the corresponding effective Hamiltonian $H_{\rm LGW}$ that is invariant under the global symmetry group of the model. For the model we consider, the microscopic order parameter is w^N and the global symmetry group is $\mathbb{Z}_q/\mathbb{Z}_N = \mathbb{Z}_p$. For $p = 2$, w^N is real and therefore, we must consider a LGW model for a scalar real field with $\mathbb{Z}_2$ global invariance. Such a model describes the standard Ising behavior. For $p > 2$, w^N is a complex number, so that the fundamental field is a complex field ψ. The effective Hamiltonian density is

$$\mathcal{H}_{\rm LGW} = \left(\sum_\mu \partial_\mu \bar{\psi} \partial_\mu \psi\right) + r|\psi|^2 + u|\psi|^4 + g_p(\psi^p + \bar{\psi}^p) + \ldots \tag{23}$$

For $p > 4$, the terms with coefficient g_p are irrelevant, and thus we obtain the O(2)/XY LGW model. For $p = 4$, the Hamiltonian Eq. (23) is equivalent to that of the so-called cubic model [64] for a two-component real field. A RG analysis shows that continuous transitions in this class of models belong to the XY universality class: the cubic-symmetric perturbation proportional to g_p is irrelevant [64] at the XY fixed

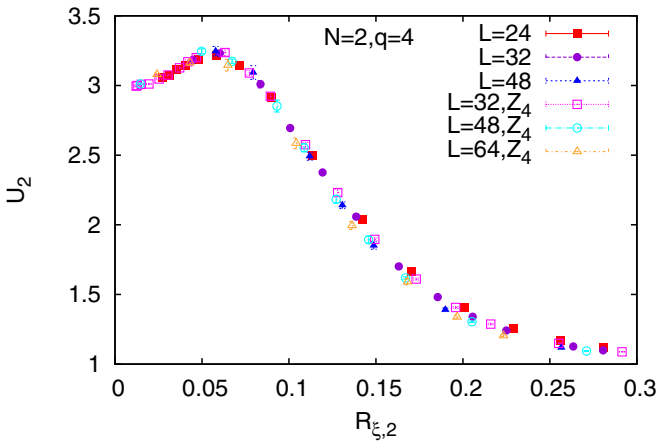

FIG. 11. Estimates of U_2 versus $R_{\xi,2}$ along the DD-OD line for $q = 4$. Results for $N = 2$ along the line $\kappa = 1$. We also report results for $\mathbb{Z}_4$ clock model.

point. For $p = 3$, the approach predicts a first-order transition because of the presence of a cubic term.

B. Large-κ transition line

We have studied the behavior along the DD-OD line for two values of N, $N = 2$, and $N = 3$. We have fixed $\kappa = 1$ and $\kappa = 1.5$ in the two cases, respectively. These two values have been chosen on the basis of the numerical estimates for the location of the topological DC-DD transition line. For $N = 2$, we have a transition at $\kappa_c \approx 0.76$, both for $\beta = 0$ (see Sec. IV) and for $\beta = 0.2$ (numerical results for $q = 6$, consistent with an Ising transition, are given in Fig. 10). For $N = 3$, we have a transition at $\kappa_c \approx 1.08$ both for $\beta = 0$ [58] and for $\beta = 0.2$ (see Fig. 10). In both cases, along the DC-DD transition line, κ is essentially constant. This guarantees us that, for the two chosen values of κ, we are considering transitions along the DC-DD line.

We have performed simulations for $(q, N) = (4, 2)$, (6,2), and (6,3) observing an ordering transition at $\beta_c = 0.4437(1)$, 0.4541(3), 0.4555(10), respectively. To further check that the transition belongs to the DD-OD line we have determined the gauge energy E_g. Close to the transition we find $E_g \approx 2.98$, 2.99 for $N = 2$ and 3, respectively; most of the plaquettes are indeed equal to 1 (for $\kappa \to \infty$ we have $E_g = 3$).

As we have discussed in Sec. IV, we expect the model to behave as the ungauged $\mathbb{Z}_q$ model. Our results are in full agreement. In Fig. 11 we report the results for U_2 versus $R_{\xi,2}$ for $q = 4$ and compare them with the analogous results for the $\mathbb{Z}_4$ model. We observe a very good agreement. Clearly, the presence of the gauge interaction is unable to destabilize the decoupled Ising behavior, as it does along the the DC-OD transition line. This result is not totally unexpected, as in the deconfined phase gauge fields are not expected to play a role (plaquettes are mostly equal to 1). In Fig. 12 we report results for the Binder parameters for $q = 6$. Since the transition in the $\mathbb{Z}_6$ clock model is in the universality class of the XY transition, one might think of comparing the scaling curves with those computed in the XY model. However, this is only possible for U_1 and U_2, but not for U_3, as discussed

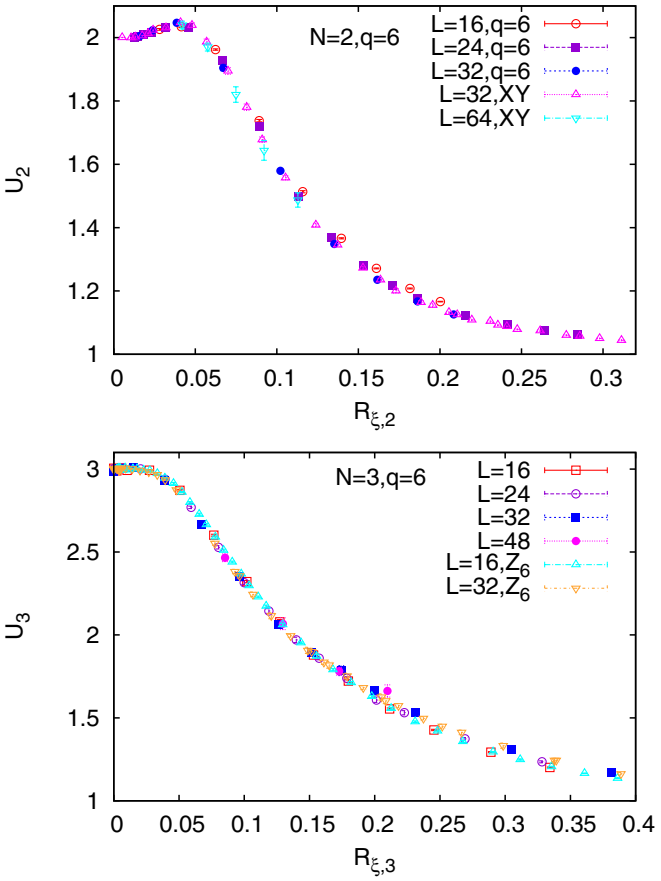

FIG. 12. Estimates of U_N versus $R_{\xi,N}$ along the DD-OD line, for $q = 6$. Resulta for $N = 2$ along the line $\kappa = 1$ (top), and for $N = 3$ along the line $\kappa = 1.5$ (bottom). In the upper panel we also report results for the XY model, in the lower panel for the $\mathbb{Z}_6$ clock model.

in Appendix C. Therefore, the results for U_3 obtained in the gauge-scalar model are directly compared with the $\mathbb{Z}_6$ results. In all cases, we observe very good agreement, confirming the irrelevance of the gauge coupling along the DD-OD line

VI. CONCLUSIONS

In this work we have studied a gauge-Higgs model with discrete scalar fields and $\mathbb{Z}_N$ gauge invariance. It is obtained by gauging the $\mathbb{Z}_N$ subgroup of the global invariance group of the $\mathbb{Z}_q$ clock model (N is a submultiple of q), in which the scalar fields are phases that take the q values $\exp(2\pi in/q)$, $n = 0, \ldots q - 1$. The resulting model is invariant under local $\mathbb{Z}_N$ and global $\mathbb{Z}_q/\mathbb{Z}_N = \mathbb{Z}_p$ ($p = q/N$) transformations. The phase diagram of the model is reported in Fig. 1. There are three different transition lines. On one line one expects the topological transitions that characterize the pure gauge $\mathbb{Z}_N$ theory. We have studied in detail the behavior of the model along the other two transition lines, along which the scalar field orders. A summary of the models investigated is reported in Table I.

The critical behavior along the small-κ transition line that separates the disordered-confined phase from the ordered-deconfined phase turns out to be in full agreement with the predictions of the Landau-Ginzburg-Wilson approach.

TABLE I. Summary of the results. For each q, N, and κ we report the critical value β_c and the universality class of the transition (last column). Along the DC-OD transition line, as q increases at fixed N, β_c is essentially independent of q for $p = q/N \geqslant 4$. Along the DD-OD line, β_c is little dependent on q, N, and κ.

q	N	κ	β_c	
		DC-OD transition line		
4	2	0.4	≈ 0.70	First order
6	2	0.4	≈ 0.875	First order
8	2	0.4	0.8869(1)	XY
10	2	0.4	0.8869(2)	XY
6	3	0.4	1.4546(1)	Ising
9	3	0.4	≈ 1.89	First order
12	3	0.4	1.9160(15)	XY
15	3	0.4	1.9150(15)	XY
10	5	0.4	4.5660(1)	Ising
		DD-OD transition line		
4	2	1.0	0.4437(1)	$\mathbb{Z}_4$/Ising
6	2	1.0	0.4541(3)	XY
6	3	1.5	0.4555(10)	XY

Criticality depends only on the global $\mathbb{Z}_p$ symmetry group of the effective theory, so that the model behaves as a ferromagnetic system with a one component complex field and $\mathbb{Z}_p$ global invariance. We thus predict that continuous transitions belong to the Ising universality class for $p = 2$ and to the O(2) universality class for any $p \geqslant 4$, the $\mathbb{Z}_p$ breaking terms being dangerously irrelevant perturbations. For $p = 3$ instead only first-order transitions are possible. Numerical data confirm these predictions quite precisely. In particular, we verify that symmetry enlargement occurs at the transition, as in the standard clock model. The condition $q \geqslant 4$ is now replaced by $p = q/N \geqslant 4$, consistently with the idea that p counts the effective number of degrees of freedom per site.

It is interesting to remark that a similar result was obtained for a very different quantum system in Ref. [43]. These authors considered a one-dimensional quantum chain with $\mathbb{Z}_6$ parafermions and showed that, by gauging a subgroup of the symmetry group, one could change the nature of the topological continuous transition. They verified numerically that, in the presence of $\mathbb{Z}_N$ ($N = 2, 3$) gauge fields, the transition belonged to the universality class of the $\mathbb{Z}_p$-invariant ($p = q/N$, with $q = 6$) two-dimensional classical spin models (the Ising model and the three-state Potts model for $p = 2$ and 3, respectively). These conclusions are in full agreement with our results.

For large κ, the OD-DD line separates two phases, in which the gauge fields are deconfined, see Fig. 1. On this line, gauge fields do not play any role (modulo gauge transformations, we have $\sigma_{x,\mu} = 1$ on most of the links), and the model behaves as the $\mathbb{Z}_q$ clock model, irrespective of the values of N.

APPENDIX A: RELATION BETWEEN THE $\mathbb{Z}_4$ MODEL WITH $\mathbb{Z}_2$ GAUGE INVARIANCE AND THE ISING MODEL

In this Appendix, we relate the $\mathbb{Z}_4$ model with $\mathbb{Z}_2$ gauge invariance with an Ising system. We rewrite $w_{\boldsymbol{x}} = e^{i\theta_{\boldsymbol{x}}}$ and parametrize the field in terms of two Ising spins $\tau_{\boldsymbol{x}}^{(1)}$ and $\tau_{\boldsymbol{x}}^{(2)}$, as

$$\cos\theta_{\boldsymbol{x}} = \tfrac{1}{2}\big(\tau_{\boldsymbol{x}}^{(1)} + \tau_{\boldsymbol{x}}^{(2)}\big), \quad \sin\theta_{\boldsymbol{x}} = \tfrac{1}{2}\big(\tau_{\boldsymbol{x}}^{(1)} - \tau_{\boldsymbol{x}}^{(2)}\big). \tag{A1}$$

In terms of the Ising spins, the Hamiltonian $H_{\rm kin}$ becomes

$$\frac{1}{T}H_{\rm kin} = -\frac{\beta}{2}\sum_{\boldsymbol{x}\mu}\big(\tau_{\boldsymbol{x}}^{(1)}\tau_{\boldsymbol{x}+\hat{\mu}}^{(1)} + \tau_{\boldsymbol{x}}^{(2)}\tau_{\boldsymbol{x}+\hat{\mu}}^{(2)}\big)\sigma_{\boldsymbol{x},\hat{\mu}}, \tag{A2}$$

which shows that the model is equivalent to two Ising systems coupled by the gauge field. Correspondingly, the correlation functions $G_Q(\boldsymbol{x}, \boldsymbol{y})$ become

$$\begin{aligned} G_1(\boldsymbol{x}, \boldsymbol{y}) &= \tfrac{1}{2}\big\langle \tau_{\boldsymbol{x}}^{(1)}\tau_{\boldsymbol{y}}^{(1)} + \tau_{\boldsymbol{x}}^{(2)}\tau_{\boldsymbol{y}}^{(2)}\big\rangle, \\ G_2(\boldsymbol{x}, \boldsymbol{y}) &= \big\langle \tau_{\boldsymbol{x}}^{(1)}\tau_{\boldsymbol{x}}^{(2)}\tau_{\boldsymbol{y}}^{(1)}\tau_{\boldsymbol{y}}^{(2)}\big\rangle. \end{aligned} \tag{A3}$$

In the absence of the gauge fields, i.e., in the $\mathbb{Z}_4$ clock model, the two Ising models decouple, and $G_1(\boldsymbol{x}, \boldsymbol{y})$ corresponds to the two-point function in the Ising model. In the same limit, the Binder parameter U_1 satisfies

$$U_1 = \tfrac{1}{2}U_{\rm Is} + \tfrac{1}{2}, \tag{A4}$$

where $U_{\rm Is}$ is the Binder parameter in the Ising model.

For $\kappa \to 0$, the gauge fields can be integrated out. If a and b can only take the values ± 1, then we can easily prove the identity

$$\sum_{\sigma=\pm 1} e^{Ka\sigma}\, e^{Kb\sigma} = 2\cosh^2 K + 2ab\sinh^2 K. \tag{A5}$$

If we define $\tilde{\beta}$ and A as

$$\tanh\tilde{\beta} = \tanh^2\frac{\beta}{2}, \quad A = 2\left(\cosh^2\frac{\beta}{2} + \sinh^2\frac{\beta}{2}\right)^{1/2}, \tag{A6}$$

and a new Ising spin $\rho_{\boldsymbol{x}} = \tau_{\boldsymbol{x}}^{(1)}\tau_{\boldsymbol{x}}^{(2)}$, then we can rewrite the partition function as

$$Z = A^{3L}2^L\sum_{\rho_x} e^{-\tilde{\beta}\,H_{\rm eff}}, \quad H_{\rm eff} = -\sum_{\boldsymbol{x},\mu}\rho_{\boldsymbol{x}}\rho_{\boldsymbol{x}+\hat{\mu}}. \tag{A7}$$

We have thus obtained an Ising model for a single spin variable at inverse temperature $\tilde{\beta}$, The mapping allows us to compute the critical temperature. Using $\tilde{\beta}_c = 0.221654626(5)$ [59], we obtain $\beta_c = 1.01246856(1)$.

The phase diagram of the model is reported in Fig. 13. As discussed in the text, a tricritical point occurs on the DC-OD line. Little is known on the behavior of the other two transition lines close to the multicritical point. The simulated points at $\beta = 0.2$ (DC-DD line) and at $\kappa = 1$ (DD-OD line) are consistent with an Ising transition.

APPENDIX B: THE $\mathbb{Z}_8$ MODEL WITH $\mathbb{Z}_2$ GAUGE INVARIANCE

One can generalize the considerations of Appendix A to the $\mathbb{Z}_8$ clock model. In this case the field $w_{\boldsymbol{x}} = e^{i\theta_{\boldsymbol{x}}}$ can be parametrized in terms of three Ising spins $\tau_{\boldsymbol{x}}^{(i)}$, $i = 1, 2, 3$, so that

$$\begin{aligned} \cos\theta_{\boldsymbol{x}} = {} & \frac{1}{8}\big(\tau_{\boldsymbol{x}}^{(1)} + \tau_{\boldsymbol{x}}^{(2)}\big)\big[2 + \sqrt{2} - (2 - \sqrt{2})\tau_{\boldsymbol{x}}^{(3)}\big] \\ & - \frac{\sqrt{2}}{8}\big(\tau_{\boldsymbol{x}}^{(1)} - \tau_{\boldsymbol{x}}^{(2)}\big)\big(1 + \tau_{\boldsymbol{x}}^{(3)}\big), \end{aligned}$$

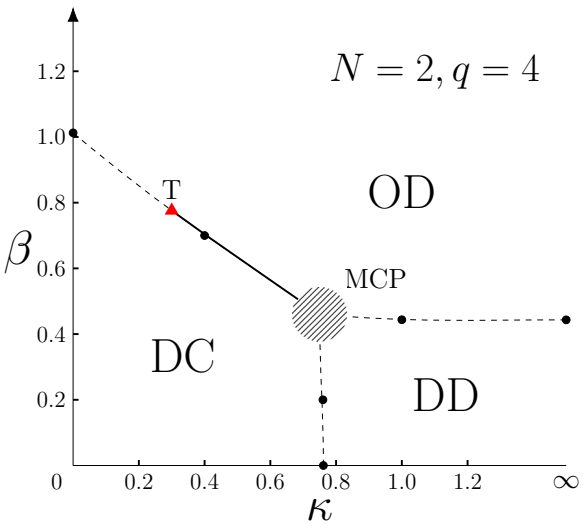

FIG. 13. Phase diagram for $q = 4$ and $N = 2$. Along the DC-OD line, the transitions belong to the Ising universality class for $\kappa < \kappa^*$ and are of first order for $\kappa > \kappa^*$ up to the multicritical point (MCP). We have no estimates of the tricritical point (located at $\kappa = \kappa^*$ along the DC-OD line, red triangle in the figure): the numerical simulations suggest $0 < \kappa^* \lesssim 0.4$. The simulated points correspond to the black dots, while the lines are only meant to guide the eye. We note that the three transition lines end at $\kappa = 0$, $\beta = 1.01246856(1)$ (DC-OD line), $\kappa = \infty$, $\beta = 0.443309252(10)$ (DD-OD line), and $\kappa = 0.761413292(12)$, $\beta = 0$ (topological DC-DD transition line).

$$\sin\theta_x = \frac{1}{8}\left(\tau_x^{(1)} - \tau_x^{(2)}\right)\left[2 + \sqrt{2} - (2-\sqrt{2})\tau_x^{(3)}\right] + \frac{\sqrt{2}}{8}\left(\tau_x^{(1)} + \tau_x^{(2)}\right)\left(1 + \tau_x^{(3)}\right). \tag{B1}$$

Under a gauge transformation $w_x \to -w_x$, the three Ising spins transform as

$$\tau_x^{(1)} \to -\tau_x^{(1)}, \quad \tau_x^{(2)} \to -\tau_x^{(2)}, \quad \tau_x^{(3)} \to \tau_x^{(3)}. \tag{B2}$$

Using this parametrization, we can rewrite

$$\cos(\theta_x - \theta_y) = \left(\tau_x^{(1)}\tau_y^{(1)} + \tau_x^{(2)}\tau_y^{(2)}\right)\left(a + b\tau_x^{(3)}\tau_y^{(3)}\right) + c\left(\tau_x^{(3)} - \tau_y^{(3)}\right)\left(\tau_y^{(1)}\tau_x^{(2)} - \tau_x^{(1)}\tau_y^{(2)}\right), \tag{B3}$$

where

$$a = \frac{1}{4\sqrt{2}}(\sqrt{2}+1), \quad b = \frac{1}{4\sqrt{2}}(\sqrt{2}-1), \quad c = \frac{1}{4\sqrt{2}}. \tag{B4}$$

Let us now consider the model in the presence of a $\mathbb{Z}_2$ gauge field σ. At $\kappa = 0$ we can integrate out the gauge field. We compute

$$Z_{x,y} = \sum_{\sigma=\pm1} e^{\beta\sigma\cos(\theta_x - \theta_y)}, \tag{B5}$$

obtaining

$$Z_{x,y} = 2\cosh^2\beta a \cosh^2\beta b \cosh^4\beta c (1 + A_1 + A_2\tau_x^{(3)}\tau_y^{(3)} + A_3\tau_x^{(1)}\tau_y^{(1)}\tau_x^{(2)}\tau_y^{(2)} + A_4\tau_x^{(1)}\tau_y^{(1)}\tau_x^{(2)}\tau_y^{(2)}\tau_x^{(3)}\tau_y^{(3)}), \tag{B6}$$

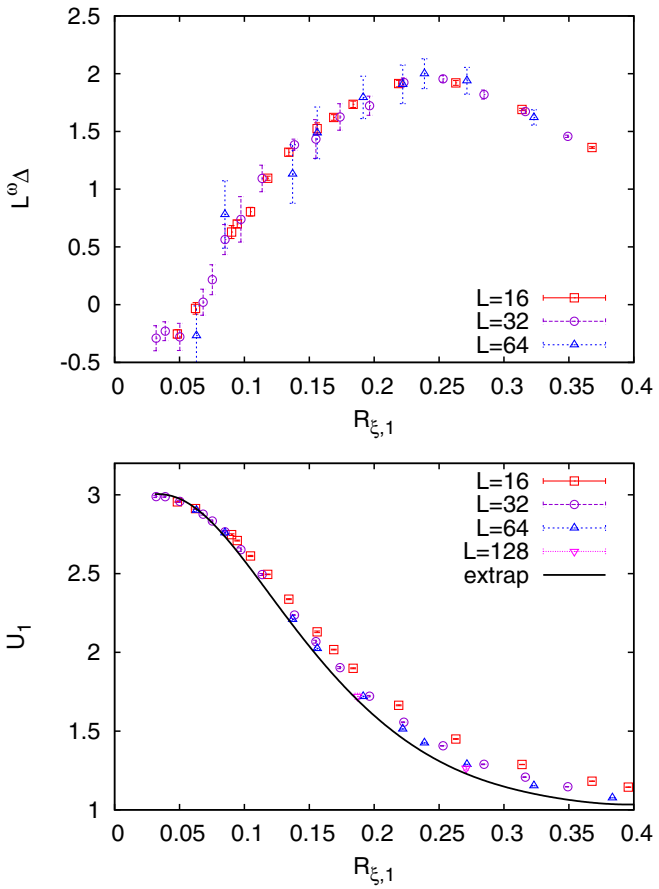

FIG. 14. Bottom: Data of U_1 versus $R_{\xi,1}$ for the Ising model and extrapolated scaling function $F_{\xi,1}(R_{\xi,1})$ ("extrap"). Top: Plot of $L^\omega\Delta$ versus $R_{\xi,1}$, where Δ is defined in Eq. (22) and $\omega = 0.83$.

where

$$\begin{aligned} A_1 &= -2\left(t_a^2 + t_b^2\right)t_c^2 + t_a^2 t_b^2\left(1 + t_c^4\right) + t_c^4, \\ A_2 &= 2t_a t_b\left(1 - t_c^2\right)^2 - 2t_c^2\left(1 - t_a^2\right)\left(1 - t_b^2\right), \\ A_3 &= \left(t_a^2 + t_b^2\right)\left(1 + t_c^4\right) - 2t_c^2\left(1 + t_a^2 t_b^2\right), \\ A_4 &= 2t_a t_b\left(1 - t_c^2\right)^2 + 2t_c^2\left(1 - t_a^2\right)\left(1 - t_b^2\right), \end{aligned} \tag{B7}$$

and we have defined $t_a = \tanh\beta a, \ldots$ An important property of the result is the relation $A_3 = A_4$, which is not apparent from the previous expressions. To prove it, it is necessary to express t_a and t_b in terms of t_c and t_d, where $d = 1/4$. We end up with

$$A_3 = A_4 = \frac{2\left(1 - t_c^2\right)^4 t_d^2}{\left(1 - t_c^2 t_d^2\right)^2}. \tag{B8}$$

Equation (B6) shows that the model can be parametrized in terms of two Ising fields. We define

$$\rho_x^{(1)} = \tau_x^{(1)}\tau_x^{(2)}\tau_x^{(3)}, \quad \rho_x^{(2)} = \tau_x^{(1)}\tau_x^{(2)}, \tag{B9}$$

obtaining the relation

$$Z_{x,y} = K\left[1 + A_1 + A_2\rho_x^{(1)}\rho_y^{(1)}\rho_x^{(2)}\rho_y^{(2)} + A_3\left(\rho_x^{(1)}\rho_y^{(1)} + \rho_x^{(2)}\rho_y^{(2)}\right)\right], \tag{B10}$$

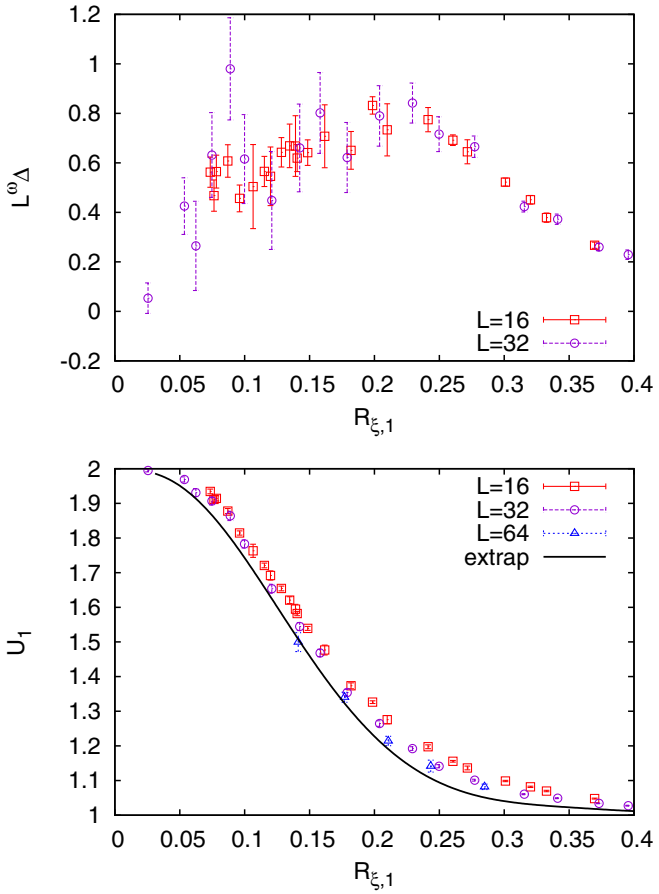

FIG. 15. Bottom: Data of U_1 versus $R_{\xi,1}$ for the $\mathbb{Z}_{20}$ model and extrapolated scaling function $F_{\xi,1}(R_{\xi,1})$. Top: Plot of $L^\omega\Delta$ versus $R_{\xi,1}$ where Δ is defined in Eq. (22) and $\omega = 0.789$ is the correction-to-scaling exponent for the XY universality class [49].

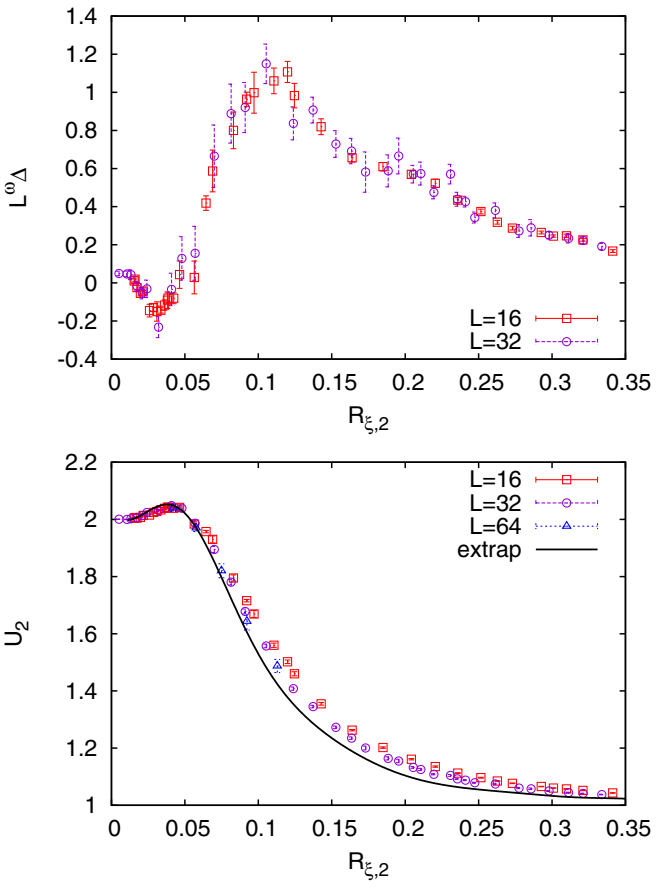

FIG. 16. Bottom: Estimates of U_2 versus $R_{\xi,2}$ for the $\mathbb{Z}_{20}$ model and extrapolated scaling function $F_{\xi,2}(R_{\xi,2})$. Top: $L^\omega\Delta$ versus $R_{\xi,2}$ where Δ is defined in Eq. (22) and $\omega = 0.789$ is the correction-to-scaling exponent for the XY universality class [49].

where K is a constant. Since $A_3^2 \neq A_2(1+A_1)$, we obtain two Ising models interacting by means of an energy-energy term. Moreover, the model is symmetric under the exchange of the two fields. In terms of the fields $\rho^{(i)}$, the $Q = 2$ correlation function takes a very simple form:

$$G_2(\boldsymbol{x},\boldsymbol{y}) = \tfrac{1}{2}\langle \rho_{\boldsymbol{x}}^{(1)}\rho_{\boldsymbol{y}}^{(1)} + \rho_{\boldsymbol{x}}^{(2)}\rho_{\boldsymbol{y}}^{(2)}\rangle. \tag{B11}$$

The critical behavior of model Eq. (B10) is well known [64]. The decoupled Ising fixed point (the one that controls the behavior of the $\mathbb{Z}_4$ clock model) is unstable. If the transition is continuous, then it is controlled by the XY fixed point.

APPENDIX C: ISING AND *XY* SCALING FUNCTIONS FOR OPEN BOUNDARY CONDITIONS

As we have discussed in the text, depending on the values of N and q, we expect to observe either Ising or XY behavior in all cases in which the transition is continuous. To determine the Ising scaling curve for U_1 as a function of $R_{\xi,1}$ we have performed runs on lattices of size $L = 16, 32, 64, 128$, determining U_1 and ξ_1. The results are shown in the lower panel of Fig. 14. Scaling corrections are significant and thus, to obtain the asymptotic scaling function $F_{\xi,1}(R_{\xi,1})$, we need to perform a fit including scaling corrections. We fit the data to Eq. (18), parametrizing the functions $F(x)$ and $F_c(x)$ with polynomials in x. We fix $\omega = 0.83$, which is the value predicted for the Ising universality class in Refs. [57,61]. The resulting curve is reported in the lower panel of Fig. 14. To verify the quality of the result, we have considered the deviations Δ defined in Eq. (22). In the upper panel of Fig. 14, we report $L^\omega\Delta$. The data scale nicely on a single curve with good precision, confirming that our estimate of the asymptotic scaling function $F_{\xi,1}(R_{\xi,1})$ is reliable and providing us with an estimate of the correction-to-scaling function $F_{c,\xi,1}(R_{\xi,1})$. Note that this function is universal apart from a multiplicative rescaling, and thus we expect scaling corrections to increase monotonically up to $R_{\xi,1} \approx 0.25$ in all models that belong to the Ising universality class. We have also determined the value of $R_{\xi,1}$ and U_1 at the critical point, by performing combined fits of the two quantities to

$$R = f(X) + L^{-\omega} f_c(X), \quad X = (\beta - \beta_c)L^{1/\nu}, \tag{C1}$$

using $\beta_c = 0.221654626(5)$ [59] and $\nu = 0.629971(4)$ [57]. We obtain

$$U_1^* = 2.72(2), \quad R_{\xi,1}^* = 0.086(1). \tag{C2}$$

These results apply to cubic-symmetric lattices with open boundary conditions. They are significantly different from

those for periodic boundary conditions: in this case, for instance, $U_1^* = 1.60356(15)$ [59].

Let us now discuss the computation of the scaling functions that express U_Q as a function of $R_{\xi,Q}$ for the XY universality class. To speed up the calculation, we have considered the $\mathbb{Z}_{20}$ clock model and we have performed extensive simulations on lattices of size up to $L = 64$. We report here the calculation of the scaling functions for $Q = 1$ and $Q = 2$. Also in this case, corrections to scaling are sizable, and therefore we have applied the same strategy used in the Ising case. The scaling functions have been parametrized using polynomials and we have used $\omega = 0.789$ [49]. Results are reported in Figs. 15 and 16, together with a scaling plot of the deviations. Deviations scale nicely, confirming the reliability of the asymptotic cirves. We have also determined the values of the two parameters at the transition:

$$U_1^* = 1.84(2), \quad R_{\xi,1}^* = 0.087(2), \tag{C3}$$

$$U_2^* = 2.02(1), \quad R_{\xi,2}^* = 0.022(2). \tag{C4}$$

The results we have obtained for the Ising and XY model are the relevant ones that shall be compared with the numerical data for the gauge-scalar model. There are, however, a few subtleties that should be taken into account.

First, in the $\mathbb{Z}_4$ clock model, although the transition belongs to the Ising universality class, the relation between $\mathbb{Z}_4$ and Ising correlation functions and Binder parameters is not trivial, as discussed in Appendix A. Relation Eq. (A4) allows us to relate the Binder parameter U_1 in the $\mathbb{Z}_4$ model in terms of the Ising Binder parameter. We have also determined the $\mathbb{Z}_4$ Binder parameter U_2 and $R_{\xi,2}$ that are associated with Ising replica correlations. At the critical point, performing the same analysis we did in the Ising case, we obtain

$$U_2^* = 3.09(1), \quad R_{\xi,2}^* = 0.032(1). \tag{C5}$$

For $q \geqslant 5$, the transition in the $\mathbb{Z}_q$ clock model belongs to the XY universality class. However, this does not imply that all correlation functions $G_Q(\boldsymbol{x}, \boldsymbol{y})$ are the same in the $\mathbb{Z}_q$ clock model and in the XY model. For instance, in the $\mathbb{Z}_q$ model we have the relations

$$G_Q(\boldsymbol{x}, \boldsymbol{y}) = G_{Q'}(\boldsymbol{x}, \boldsymbol{y}), \quad Q' = |Q - nq|, \tag{C6}$$

for any integer n. These relations do not hold in the XY model. Similar relations hold for the Binder parameters U_Q. We have studied this issue in the $\mathbb{Z}_6$ clock model, verifying in this case that the scaling function of U_Q versus $R_{\xi,Q}$ is the same in the $\mathbb{Z}_6$ and in the XY model for $Q = 1, 2$, while it differs for $Q = 3$. The different behavior can be easily proved by noting that, in the disordered limit ($R_{\xi,3} \to 0$), we have $U_3 = 3$, 2 in the $\mathbb{Z}_6$ model and in the XY model, respectively. Similar arguments can be used for any q, to show that U_Q differs in the $\mathbb{Z}_q$ model and in the XY model for $Q \geqslant q/2$.

[1] E. Fradkin, *Field Theories of Condensed Matter Physics*, 2nd ed. (Cambridge University Press, Cambridge, UK, 2013).

[2] R. Moessner and J. E. Moore, *Topological Phases of Matter* (Cambridge University Press, Cambridge, UK, 2021).

[3] N. Read and S. Sachdev, Spin-Peierls, valence-bond solid, and Néel ground states of low-dimensional quantum antiferromagnets, Phys. Rev. B **42**, 4568 (1990).

[4] T. Senthil, L. Balents, S. Sachdev, A. Vishwanath, and M. P. A. Fisher, Quantum criticality beyond the Landau-Ginzburg-Wilson paradigm, Phys. Rev. B **70**, 144407 (2004).

[5] S. Takashima, I. Ichinose, and T. Matsui, CP^1+U(1) lattice gauge theory in three dimensions: Phase structure, spins, gauge bosons, and instantons, Phys. Rev. B **72**, 075112 (2005).

[6] S. Takashima, I. Ichinose, and T. Matsui, Deconfinement of spinons on critical points: Multiflavor CP^1+U(1) lattice gauge theory in three dimension, Phys. Rev. B **73**, 075119 (2006).

[7] R. K. Kaul, Quantum phase transitions in bilayer SU(N) antiferromagnets, Phys. Rev. B **85**, 180411(R) (2012).

[8] R. K. Kaul and A. W. Sandvik, Lattice Model for the SU(N) Néel to Valence-Bond Solid Quantum Phase Transition at Large N, Phys. Rev. Lett. **108**, 137201 (2012).

[9] T. A. Bojesen and A. Sudbø, Berry phases, current lattices, and suppression of phase transitions in a lattice gauge theory of quantum antiferromagnets, Phys. Rev. B **88**, 094412 (2013).

[10] M. S. Block, R. G. Melko, and R. K. Kaul, Fate of CP^{N-1} Fixed Point With q Monopoles, Phys. Rev. Lett. **111**, 137202 (2013).

[11] A. Nahum, J. T. Chalker, P. Serna, M. Ortuño, and A. M. Somoza, Deconfined Quantum Criticality, Scaling Violations, and Classical Loop Models, Phys. Rev. X **5**, 041048 (2015).

[12] C. Wang, A. Nahum, M. A. Metliski, C. Xu, and T. Senthil, Deconfined Quantum Critical Points: Symmetries and Dualities, Phys. Rev. X **7**, 031051 (2017).

[13] S. Sachdev, Topological order, emergent gauge fields, and Fermi surface reconstruction, Rep. Prog. Phys. **82**, 014001 (2019).

[14] E. Fradkin and S. H. Shenker, Phase diagrams of lattice gauge theories with Higgs fields, Phys. Rev. D **19**, 3682 (1979).

[15] K. C. Bowler, G. S. Pawley, B. J. Pendleton, and D. J. Wallace, Phase diagrams of U(1) lattice Higgs models, Phys. Lett. B **104**, 481 (1981).

[16] A. Pelissetto and E. Vicari, Multicomponent compact Abelian-Higgs lattice models, Phys. Rev. E **100**, 042134 (2019).

[17] C. Bonati, A. Pelissetto, and E. Vicari, Higher-charge three-dimensional compact lattice Abelian-Higgs models, Phys. Rev. E **102**, 062151 (2020).

[18] C. Bonati, A. Pelissetto, and E. Vicari, Critical behaviors of lattice U(1) gauge models and three-dimensional Abelian-Higgs gauge field theory, Phys. Rev. B **105**, 085112 (2022).

[19] A. Pelissetto and E. Vicari, Three-dimensional monopole-free CP^{N-1} models, Phys. Rev. E **101**, 062136 (2020).

[20] C. Bonati, A. Pelissetto, and E. Vicari, Three-dimensional monopole-free CP^{N-1} models: Behavior in the presence of a quartic potential, arXiv:2202.04614.

[21] A. Nahum, J. T. Chalker, P. Serna, M. Ortuño, and A. M. Somoza, 3D Loop Models and the $CP^{N-1}\sigma$ Model, Phys. Rev. Lett. **107**, 110601 (2011).

[22] A. Nahum, J. T. Chalker, P. Serna, M. Ortuño, and A. M. Somoza, Phase transitions in three-dimensional loop models and the $CP^{N-1}\sigma$ model, Phys. Rev. B **88**, 134411 (2013).

[23] C. Bonati, A. Pelissetto, and E. Vicari, Lattice Abelian-Higgs model with noncompact gauge fields, Phys. Rev. B **103**, 085104 (2021).

[24] F. J. Wegner, Duality in generalized Ising models and phase transitions without local order parameters, J. Math. Phys. **12**, 2259 (1971).

[25] J. B. Kogut, An introduction to lattice gauge theory and spin systems, Rev. Mod. Phys. **51**, 659 (1979).

[26] F. Gliozzi and A. Rago, Monopole clusters, center vortices, and confinement in a Z_2 gauge-Higgs system, Phys. Rev. D **66**, 074511 (2002).

[27] L. Genovese, F. Gliozzi, A. Rago, and C. Torrero, The phase diagram of the three-dimensional Z_2 gauge-Higgs system at zero and finite temperature, Nucl. Phys. B Proc. Suppl. **119**, 894 (2003).

[28] T. Senthil and M. P. A. Fisher, $\mathbb{Z}_2$ gauge theory of electron fractionalization in strongly correlated systems, Phys. Rev. B **62**, 7850 (2000).

[29] R. Moessner, S. L. Sondhi, and E. Fradkin, Short-ranged resonating valence bond physics, quantum dimer models, and Ising gauge theories, Phys. Rev. B **65**, 024504 (2001).

[30] R. D. Sedgewick, D. J. Scalapino, and R. L. Sugar, Fractionalized phase in an XY-Z_2 gauge model, Phys. Rev. B **65**, 054508 (2002).

[31] D. Podolsky and E. Demler, Properties and detection of spin nematic order in strongly correlated electron systems, New J. Phys. **7**, 59 (2005).

[32] Z. Nussinov, Derivation of the Fradkin-Shenker result from duality: Links to spin systems in external magnetic fields and percolation crossovers, Phys. Rev. D **72**, 054509 (2005).

[33] P. E. Lammert, D. S. Rokhsar, and J. Toner, Topology and Nematic Ordering, Phys. Rev. Lett. **70**, 1650 (1993); Topology and nematic ordering I: A gauge theory, Phys. Rev. E **52**, 1778 (1995); J. Toner, P. E. Lammert, and D. S. Rokhsar, Topology and nematic ordering. II. Observable critical behavior, *ibid.* **52**, 1801 (1995).

[34] K. Liu, J. Nissinen, Z. Nussinov, R.-J. Slager, K. Wu, and J. Zaanen, Classification of nematic order in $2+1$ dimensions: Dislocation melting in an $O(2)/\mathbb{Z}_N$ lattice gauge theory, Phys. Rev. B **91**, 075103 (2015).

[35] J. Vidal, S. Dusuel, and K. P. Schmidt, Low-energy effective theory of the toric code model in a parallel magnetic field, Phys. Rev. B **79**, 033109 (2009).

[36] I. S. Tupitsyn, A. Kitaev, N. V. Prokofev, and P. C. E. Stamp, Topological multicritical point in the phase diagram of the toric code model and three-dimensional lattice gauge-Higgs model, Phys. Rev. B **82**, 085114 (2010).

[37] F. Wu, Y. Deng, and N. Prokofev, Phase diagram of the toric code model in a parallel magnetic field, Phys. Rev. B **85**, 195104 (2012).

[38] A. Somoza, P. Serna, and A. Nahum, Self-Dual Criticality in Three-Dimensional $\mathbb{Z}_2$ Gauge Theory with Matter, Phys. Rev. X **11**, 041008 (2021).

[39] M. Grady, Exploring the 3D Ising gauge-Higgs model in exact Coulomb gauge and with a gauge-invariant substitute for Landau gauge, arXiv:2109.04560.

[40] L. Homeier, C. Schweizer, M. Aidelsburger, A. Fedorov, and F. Grusdt, $\mathbb{Z}_2$ lattice gauge theories and Kitaev's toric code: A scheme for analog quantum simulation, Phys. Rev. B **104**, 085138 (2021).

[41] C. Bonati, A. Pelissetto, and E. Vicari, Multicritical point of the three-dimensional $\mathbb{Z}_2$ gauge-Higgs model, Phys. Rev. B **105**, 165138 (2022).

[42] J. Alicea and P. Fendley, Topological phases with parafermions: Theory and blueprints, Annu. Rev. Condens. Matter Phys. **7**, 119 (2016).

[43] E. Cobanera, J. Ulrich, and F. Hassler, Changing anyonic ground degeneracy with engineered gauge fields, Phys. Rev. B **94**, 125434 (2016).

[44] J. Smiseth, E. Smørgrav, F. S. Nogueira, J. Hove, and A. Sudbø, Phase structure of $d = 2 + 1$ compact lattice gauge theories and the transition from Mott insulator to fractionalized insulator, Phys. Rev. B **67**, 205104 (2003).

[45] J. Hove and A. Sudbø, Criticality versus q in the $(2+1)$-dimensional Z_q clock model, Phys. Rev. E **68**, 046107 (2003)

[46] H. Shao, W. Guo, and A. W. Sandvik, Monte Carlo Renormalization Flows in the Space of Relevant and Irrelevant Operators: Application to Three-Dimensional Clock Models, Phys. Rev. Lett. **124**, 080602 (2020).

[47] P. Patil, H. Shao, and A. W. Sandvik, Unconventional U(1) to Z_q cross-over in quantum and classical q-state clock models, Phys. Rev. B **103**, 054418 (2021).

[48] L. Barbiero, C. Schweizer, M. Aidelsburger, E. Demler, N. Goldman, and F. Grusdt, Coupling ultracold matter to dynamical gauge fields in optical lattices: From flux attachment to Z_2 lattice gauge theories, Sci. Adv. **5**, eaav7444 (2019).

[49] M. Hasenbusch, Monte Carlo study of an improved clock model in three dimensions, Phys. Rev. B **100**, 224517 (2019).

[50] M. Hasenbusch, Monte Carlo study of a generalized icosahedral model on the simple cubic lattice, Phys. Rev. B **102**, 024406 (2020).

[51] N. Klco and M. J. Savage, Digitization of scalar fields for quantum computing, Phys. Rev. A **99**, 052335 (2019).

[52] Y. Ji, H. Lamm, and S. Zhu, Gluon field digitization via group space decimation for quantum computers, Phys. Rev. D **102**, 114513 (2020).

[53] M. S. S. Challa, D. P. Landau, and K. Binder, Finite-size effects at temperature-driven first-order transitions, Phys. Rev. B **34**, 1841 (1986).

[54] K. Vollmayr, J. D. Reger, M. Scheucher, and K. Binder, Finite size effects at thermally-driven first order phase transitions: A phenomenological theory of the order parameter distribution, Z. Phys. B **91**, 113 (1993).

[55] P. Calabrese, A. Pelissetto, and E. Vicari, Multicritical phenomena in $O(n_1) \oplus O(n_2)$ symmetric theories, Phys. Rev. B **67**, 054505 (2003).

[56] S. Pujari, F. Alet, and K. Damle, Transitions to valence-bond solid order in a honeycomb lattice antiferromagnet, Phys. Rev. B **91**, 104411 (2015)

[57] F. Kos, D. Poland, D. Simmons-Duffin, and A. Vichi, Precision islands in the Ising and $O(N)$ models, J. High. Energy Phys. 08 (2016) 036.

[58] O. Borisenko, V. Chelnokov, G. Cortese, M. Gravina, A. Papa, and I. Surzhikov, Critical behavior of 3D Z(N) lattice gauge theories at zero temperature, Nucl. Phys. B **879**, 80 (2014).

[59] A. M. Ferrenberg, J. Xu, and D. P. Landau, Pushing the limits of Monte Carlo simulations for the three-dimensional Ising model, Phys. Rev. E **97**, 043301 (2018).

[60] T. Neuhaus, A. Rajantie, and K. Rummukainen, Numerical study of duality and universality in a frozen superconductor, Phys. Rev. B **67**, 014525 (2003).

[61] S. El-Showk, M. F. Paulos, D. Poland, S. Rychkov, D. Simmons-Duffin, and A. Vichi, Solving the 3D Ising model with the conformal bootstrap, Phys. Rev. D **86**, 025022 (2012); Solving the 3D Ising Model with the Conformal Bootstrap II. *c*-Minimization and Precise Critical Exponents, J. Stat. Phys. **157**, 869 (2014).

[62] M. Campostrini, M. Hasenbusch, A. Pelissetto, E. Vicari, Theoretical estimates of the critical exponents of the superfluid transition in ^{4}He by lattice methods, Phys. Rev. B **74**, 144506 (2016).

[63] S. M. Chester, W. Landry, J. Liu, D. Poland, D. Simmons-Duffin, N. Su, and A. Vichi, Carving out OPE space and precise O(2) model critical exponents, J. High Energy Phys. 06 (2020) 142.

[64] J. M. Carmona, A. Pelissetto, and E. Vicari, *N*-component Ginzburg-Landau Hamiltonian with cubic anisotropy: A six-loop study, Phys. Rev. B **61**, 15136 (2000).